BMC Medical Imaging

RESEARCH Open Access

StrokeNeXt: an automated stroke classification model using computed tomography and magnetic resonance images

Evren Ekingen[1], Ferhat Yildirim[2], Ozgur Bayar[3], Erhan Akbal[4*], Ilknur Sercek[4], Abdul Hafeez-Baig[5], Sengul Dogan[4] and Turker Tuncer[4]

Abstract

Background and Objective Stroke ranks among the leading causes of disability and death worldwide. Timely detection can reduce its impact. Machine learning delivers powerful tools for image-based diagnosis. This study introduces StrokeNeXt, a lightweight convolutional neural network (CNN) for computed tomography (CT) and magnetic resonance (MR) scans, and couples it with deep feature engineering (DFE) to improve accuracy and facilitate clinical deployment.

Materials and Methods We assembled a multimodal dataset of CT and MR images, each labeled as stroke or control. StrokeNeXt employs a ConvNeXt-inspired block and a squeeze-and-excitation (SE) unit across four stages: stem, StrokeNeXt block, downsampling, and output. In the DFE pipeline, StrokeNeXt extracts features from fixed-size patches, iterative neighborhood component analysis (INCA) selects the top features, and a t algorithm-based k-nearest neighbors (tkNN) classifier has been utilized for classification.

Results StrokeNeXt achieved 93.67% test accuracy on the assembled dataset. Integrating DFE raised accuracy to 97.06%. This combined approach outperformed StrokeNeXt alone and reduced classification time.

Conclusion StrokeNeXt paired with DFE offers an effective solution for stroke detection on CT and MR images. Its high accuracy and fewer learnable parameters make it lightweight and it is suitable for integration into clinical workflows. This research lays a foundation for real-time decision support in emergency and radiology settings.

Keywords Stroke detection, Deep feature engineering, Patch-based feature extraction

*Correspondence:
Erhan Akbal
erhanakbal@firat.edu.tr; erhanakbal@gmail.com
[1]Department of Emergency, Etlik City Hospital, Ankara, Turkey
[2]Department of Radiology, Finike City Hospital, Antalya, Turkey
[3]Department of Emergency, Ankara Provincial Health Directorate, Mamak State Hospital, Ankara, Turkey
[4]Department of Digital Forensics Engineering, Technology Faculty, Firat University, Elazig, Turkey
[5]School of Business, University of Southern Queensland, Toowoomba Queensland, Australia

Introduction

Stroke is a major healthcare issue. It causes partial or complete loss of motor abilities in patients [1, 2]. The World Health Organization (WHO) reports that strokes affect 15 million people each year and cause 5 million deaths. Therefore, the mortality rate of stroke is very high. This condition (stroke) affects mainly people over age 40. Younger patients with high blood pressure also face this risk [3]. Major risk factors for stroke are tobacco use, alcohol intake, high blood pressure, and obesity [4, 5]. Early detection is critical. Advances in CT and MR imaging have proved vital for early detection [6]. These tools produce large datasets and require many hours of work by medical specialists for accurate diagnosis and treatment planning [7–9].

Artificial intelligence (AI) has become an admirable tool for problem solving. Therefore, AI tools have been utilized for handling biomedical challenges [10]. AI models can extract essential information from large datasets and ease the workload of healthcare professionals. Demand for more precise models remains, especially those able to detect stroke in CT and MR images with high accuracy [11]. This research presents StrokeNeXt and this convolutional neural network (CNN) model is an innovative fully convolutional lightweight model. StrokeNeXt is designed for precise stroke detection on computed tomography (CT) and magnetic resonance (MR) images in this research. This model builds on the ConvNeXt architecture and adds a squeeze-and-excitation (SE) block to improve feature representation. This study describes the design of StrokeNeXt and its novel layers and blocks.

We collected a dataset of CT and MR scans and divided the images into stroke and control classes. We tested StrokeNeXt on this dataset and measured its detection accuracy. We also used a patch-based deep feature method that uses ViT [12] elements for feature extraction, followed by feature selection [13] and classification to refine the model's predictive power.

To create the stroke datasets, MR and CT images have generally used and, the advantages and limitations of MR- and CT-based stroke detection models are:

- CT imaging costs less than MR imaging but contains less detail. CT scans are the first choice in emergency services and play a key role in early diagnosis.
- MR imaging is expensive but provides detailed information about stroke.

Literature review

There are various machine learning-based studies proposed for different disciplines in the literature [14–17]. Some recent studies on stroke detection include the following. Subudhi et al. [18] proposed a feature-engineering model for ischemic stroke detection and achieved 95.00% accuracy. This approach relies on predefined features and may not adapt well to new image data. Ozaltin et al. [19] introduced OzNet for CT image classification, selecting 250 features from its fully connected layer and reporting 98.42% accuracy. They collected a small dataset since their dataset has limited number of the images. Moreover, their presented OzNet is a simple version of the VGG. Cetinoglu et al. [20] applied a CNN to diffusion-weighted MRI images in 421 cases (271 acute stroke, 150 controls) and obtained 96.00% accuracy. The study did not include validation on other MRI modalities or external datasets. Aishvarya et al. [21] developed a system for early stroke detection in MRI images using machine learning and image processing, with accuracy above 90%. The method lacks detailed comparison with existing approaches and evaluation on diverse patient groups. Tang et al. [22] presented a computer-aided detection scheme for small lesion identification in non-enhanced CT images, testing on 101 scans and attaining an area under the ROC curve of 99.90%. The small test set limits assessment of its general performance and they only used CT images. Badriyah et al. [23] evaluated eight machine learning algorithms on CT scans from 102 patients (226 ischemic, 7 hemorrhagic images) and reached 95.97% accuracy. The severe class imbalance may affect the reliability of hemorrhage classification. Krishna et al. [24] used a dataset of 5 110 instances for early stroke detection with machine learning and reported 99.35% accuracy. The study did not specify image types or address potential overfitting. Ayoub et al. [25] proposed an developed Vision Transformer (ViT) architecture for multi-slice CT classification in 730 patients (normal, infarction, hemorrhage) and yielded 87.51% accuracy. The model shows lower performance in hemorrhage cases and offers limited lesion localization. Moreover, their utilized model is not original. Gautam et al. [26] applied a feature extractor to 900 CT images for classification into normal, ischemic, or hemorrhagic categories and obtained 82.65% accuracy. Their model has relatively low classification performance. Lee et al. [27] used a CNN on diffusion-weighted MRI slices and attained 86.30% accuracy. They only used diffusion-weighted MRI slices and MRI is an expensive process. Patel et al. [28] employed EfficientNetB0 on 100 CT images and reported 97% accuracy. The small sample size limits its generalizability and they used well-known deep learning model (EfficientNetB0). Thus, they have no contribution to deep learning. Raj et al. [29] applied machine learning to CT scans from 233 patients and reached 92.00% accuracy. They only used CT images. Other modalities can be used to test their models.

Literature gaps

According to the literature review, identified gaps include:

- Stroke is a common disorder, but public image datasets for stroke, particularly those combining MR and CT scans, are scarce. Moreover, the most of the models have used small image datasets.
- Most studies use deep learning models for stroke detection, typically relying on established CNN architectures to achieve high classification/detection accuracy.
- Since 2020, transformers have gained prominence in computer vision, and proposals for new CNN models have declined; only a few next-generation CNNs have been introduced.
- Most studies use deep learning or feature engineering for stroke detection, and very few combine both methods.

Motivation

Our essential motivation is to introduce a new CNN, StrokeNeXt, that detects strokes with high accuracy and uses fewer learnable parameters. To support this aim, we created a dataset of stroke and control cases using CT and MR images. This multimodal dataset includes both CT and MR scans. We have used stroke dataset since we aimed to show that the recommended StrokeNeXt can solve real life problems. By collecting a multimodal dataset, we aimed to fill the first literature gap and the collected dataset contains more than 5000 medical images. Also, by proposing an innovative CNN model, the second gap has been filled since the most of the biomedical image classification/detection researches have used the well-known CNN models to guarantee the high classification/detection performance. In this research, we took this risk.

Recent work in computer vision has focused on transformers such as ViT [12] and Swin Transformer [30] because of their strong classification performance. This focus has led to fewer new CNN proposals. A few new CNNs, such as ConvNeXt [31] and Hyenadna [32], still offer competitive alternatives. In this study, we enrich CNN methods by adding a novel block to StrokeNeXt. By presenting the StrokeNeXt CNN, we have filled the third literature gap.

Although several feature engineering models appear in the literature, they have lower classification accuracy than deep learning models [33–35]. Feature engineering does offer lower computational complexity and simplicity [36]. We therefore present a Deep Feature Engineering (DFE) model that uses transfer learning with StrokeNeXt to improve classification accuracy. Inspired by ViT, our DFE model uses patch-based feature extraction and aims to combine deep learning and feature engineering strengths. By recommending the StrokeNeXt-based DFE, fourth literature gap has been filled.

Innovations

The innovative aspects of the StrokeNeXt-based stroke detection research include:

- A new multimodal dataset of CT and MR images for stroke detection
- StrokeNeXt, a lightweight CNN model in deep learning
- A DFE model with patch-based feature extraction, iterative feature selection, and classification techniques.

Contributions

Our contributions are:

- Compiling a publicly available multimodal CT and MR image dataset for stroke detection to enable effective deep-learning training and support future multimodal model development.
- Developing StrokeNeXt, a novel lightweight CNN model, and a StrokeNeXt–based DFE model attained over 93% test classification accuracies. The recommended DFE increased test classification performances of the recommended StrokeNeXt. In this respect, this research contributes to both CNN and feature engineering.

The collected image dataset

Our dataset was collected retrospectively from a single medical center between 2021 and 2023 years. CT imaging was performed on a 128-slice GE Revolution scanner in the axial plane with a 5 mm slice thickness. MRI was acquired on a GE Signa 1.5 T system using axial diffusion-weighted imaging (DWI) sequences at b-values of 0 and 1000 s/mm^2. All acquisitions followed the hospital's standard stroke screening protocol. There are two distinct classes: (1) stroke and (2) control. These classes were clinically verified with neurologists and neuroradiologists. The dataset comprises data from 230 participants, with a gender distribution of 113 females and 117 males. Among these participants, 115 were diagnosed with stroke, while the remaining 115 were categorized under the control group. An average of 7–8 cross-sectional images were used for each imaging type. The dataset includes a total of 5,336 CT and MRI (2226 CT + 3110 MR) images, with 2,695 images representing stroke cases and 2,641 images corresponding to control cases. This dataset was collected retrospectively from a medical center. We obtained ethical approval from the Non-Invasive Ethics Committee of the Ankara Provincial Health

Directorate at Yıldırım Beyazıt University Yenimahalle Training and Research Hospital on December 7, 2023 (E-2023-76).

All patient imaging data were fully anonymized before analysis. Identifiers such as name, date of birth, patient ID, and acquisition timestamps were removed from all image headers. We reviewed the dataset for missing images or labels and excluded any cases with incomplete CT or MR series; no imputation was performed. Reference labels were assigned by one neuroradiologist and two emergency medicine specialists, based on clinical reports and follow-up data.

The distribution of the collected multimodal image dataset has been given in Table 1.

As shown in Table 1, the final dataset comprises 5,336 images (2,226 CT and 3,110 MR) from 230 patients (115 stroke, 115 control; 113 females, 117 males). Each patient contributed an average of 7–8 cross-sectional images per modality. Patient ages ranged from 19 to 91 years (mean 61.63).

We split the data at the patient level to avoid overlap. Stratified sampling preserved the stroke/control ratio: ~75% of patients (173) and 4,009 images went to the training set; ~25% of patients (57) and 1,327 images formed the test set. The test set size was chosen to achieve over 80% power to detect a 3% difference in accuracy ($\alpha = 0.05$).

To create the validation set, we randomly selected 30% of the training images. This yields 2,806 training, 1,203 validations, and 1,327 test images. The resulting split ratio for training, validation, and test sets is approximately 52.5: 22.5: 25.

Moreover, this dataset was publicly published on the web and the users can download this dataset utilizing https://www.kaggle.com/datasets/turkertuncer/multimodal-stroke-image-dataset URL.

StrokeNeXt

This research introduces StrokeNeXt, an innovative CNN model for stroke image analysis. StrokeNeXt uses fewer than 10 million learnable parameters (about 7.3 million). Therefore, the presented version of the StrokeNeXt is lightweight. Its architecture consists of four phases: stem, StrokeNeXt block, downsampling, and output block. The StrokeNeXt block, a key innovation, appears in Fig. 1.

As illustrated in Fig. 1, the process begins with pixel-wise convolution, increasing the number of filters by six-fold. Subsequently, batch normalization is applied to normalize the outputs. This block follows a sequence of operations similar to ConvNeXt, involving convolution, normalization, another convolution, activation, a further convolution, and then normalization again. For the second convolution operation, a 3×3 convolution is utilized with the same number of filters, accompanied by GELU activation. Following this, a squeeze-and-excitation (SE) block is incorporated to enhance the block's focus on relevant features. The final convolution step again employs pixel-wise convolution and batch normalization. Additionally, a shortcut connection, reminiscent of residual blocks, is used to mitigate the vanishing gradient problem. The mathematical formulation of this block is detailed below.

$$X_t = BN\left(C_F^{1\times1}\left(SE_{\frac{1}{6}}\left(GELU\left(C_{6F}^{3\times3}\left(BN\left(C_{6F}^{1\times1}\left(X_{t-1}\right)\right)\right)\right)\right)\right)\right) + X_{t-1} \quad (1)$$

where $C_y^x(.)$: convolution operator and x define the filter size, and y represent the number of filters. Moreover, X_t: the output of the t[th] time. Also, we have defined $SE(.)$ function below.

$$SE_{\frac{1}{6}}(S_{t-1}) = S_t = Sigmoid\left(C_{6F}^{1\times1}\left(GELU\left(C_F^{1\times1}\left(GAP\left(S_{t-1}\right)\right)\right)\right)\right) \times S_{t-1} \quad (2)$$

Herein, S_{t-1}: input of the SE block/function and S_t: output of the SE block.

Table 1 Distribution of the collected CT and MR image dataset

No	Number of participants	Demographic characteristics of patients	Class	Train	Test	Total
1	Female:59 Male:56 Total:115	*Female:* Min:25, Average: 59.78, Max: 78 *Male:* Min: 24, Average:61.14, Max:82 *Overall:* Min:24, Average: 60.47, Max: 82	Stroke	CT: 699, MR: 1326, Total: 2025	CT: 230, MR: 440, Total: 670	2695
2	Female:60 Male:55 Total:115	*Female:* Min:21, Average: 63.04, Max: 88 *Male:* Min:19, Average:59.78, Max: 91 *Overall:* Min: 19, Average:62.28, Max:91	Control	CT: 975, MR: 1009, Total: 1984	CT: 322, MR: 335, Total: 657	2641
Total	Female:119 Male:111 Total:230	Min:19, Average: 61.63, Max:91		4009	1327	5336

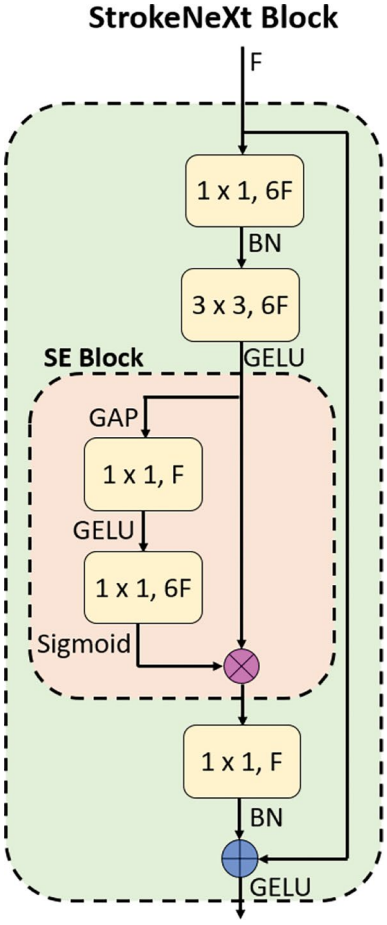

Fig. 1 The proposed StrokeNeXt block. Herein, F: number of filters, BN: Batch Normalization, GELU: Gaussian Error Linear Unit, GAP: Global Average Pooling

By implementing the proposed block, we have introduced the StrokeNeXt CNN model and a graphical representation of StrokeNeXt is depicted in Fig. 2.

To develop this model (StrokeNeXt), we were inspired by the structure of MobileNet, which begins with a small number of filters that increase toward the output block. Consequently, we started with 48 filters for the stem block. We utilized the proposed StrokeNeXt block in a repetitive structure in the main block. For downsampling, patchify average pooling was employed to reduce the tensor size, while pixel-wise convolution was used to increase the number of filters. In the output block, we applied two convolutions with 640 and 1024 filters, respectively, adhering to the ConvNeXt paradigm (convolution + BN + convolution + GELU). By implementing Global Average Pooling (GAP), we obtained the final feature map and determined the number of classes in the fully connected layer. Finally, a Softmax function was used to generate classification results. The mathematical specifics of StrokeNeXt are detailed in Table 2.

As detailed in Table 2, our proposed StrokeNeXt model comprises approximately 7.3 million parameters, classifying it as a lightweight CNN model. The various phases of the model are explained as follows.

Stem Layer: The initial processing phase begins with images sized at 224×224 pixels across three color channels (RGB). Therefore, the size of the input image is $224 \times 224 \times 3$. It undergoes two convolutional operations: the first with a 7×7 kernel featuring 24 filters, batch normalization (BN), GELU activation, and a stride of 2, followed by a second convolution using a 3×3 kernel with 48 filters, also with BN and GELU activation, and a stride of 2. This results in a feature map sized at 56×56 pixels with 48 channels.

Main Block 1: Receiving the output from the stem layer, this block executes a sequence of operations twice. It starts with a 1×1 convolution to expand the channel depth to 288, followed by a 3×3 convolution with the same number of filters that incorporates a squeeze-and-excitation (SE) block for improved feature selection, and concludes with another 1×1 convolution to revert the channel count back to 48. This process maintains the feature map size at 56×56 pixels with 48 channels.

Downsampling 1: This stage takes the feature map from Main Block 1 and applies average pooling with a 2×2 kernel and stride of 2, reducing the spatial dimensions. A subsequent 1×1 convolution increases the depth to 96 channels, further processed by BN and GELU activation, resulting in a 28×28 pixels feature map with 96 channels.

Main Blocks 2 to 4 and Downsampling Phases: Following the pattern established in Main Block 1 and Downsampling 1, each successive block and downsampling phase refines the feature map's size and depth as per their specific operations. Notably, the final downsampling phase (Downsampling 3) reduces the feature map to 7×7 pixels with 384 channels.

Output Phase: The model's final phase processes the $7 \times 7 \times 384$ feature map from Main Block 4, utilizing a 1×1 convolution to increase the channel depth to 640, then to 1280 with BN and GELU activation. Global Average Pooling (GAP) condenses each 7×7 channel to a singular feature, which feeds into a fully connected layer equipped with Softmax for classification. This yields the classification scores for the model's designated classes, marking the culmination of the model's intricate processing pathway to achieve its classification objectives.

StrokeNeXt-based deep feature engineering

We have introduced a novel DFE model leveraging the proposed StrokeNeXt. This DFE model encompasses three primary phases: (i) patch-based feature extraction, (ii) feature selection based on INCA [37], and (iii) classification using. A graphical overview of the StrokeNeXt-based DFE model is provided in Fig. 3.

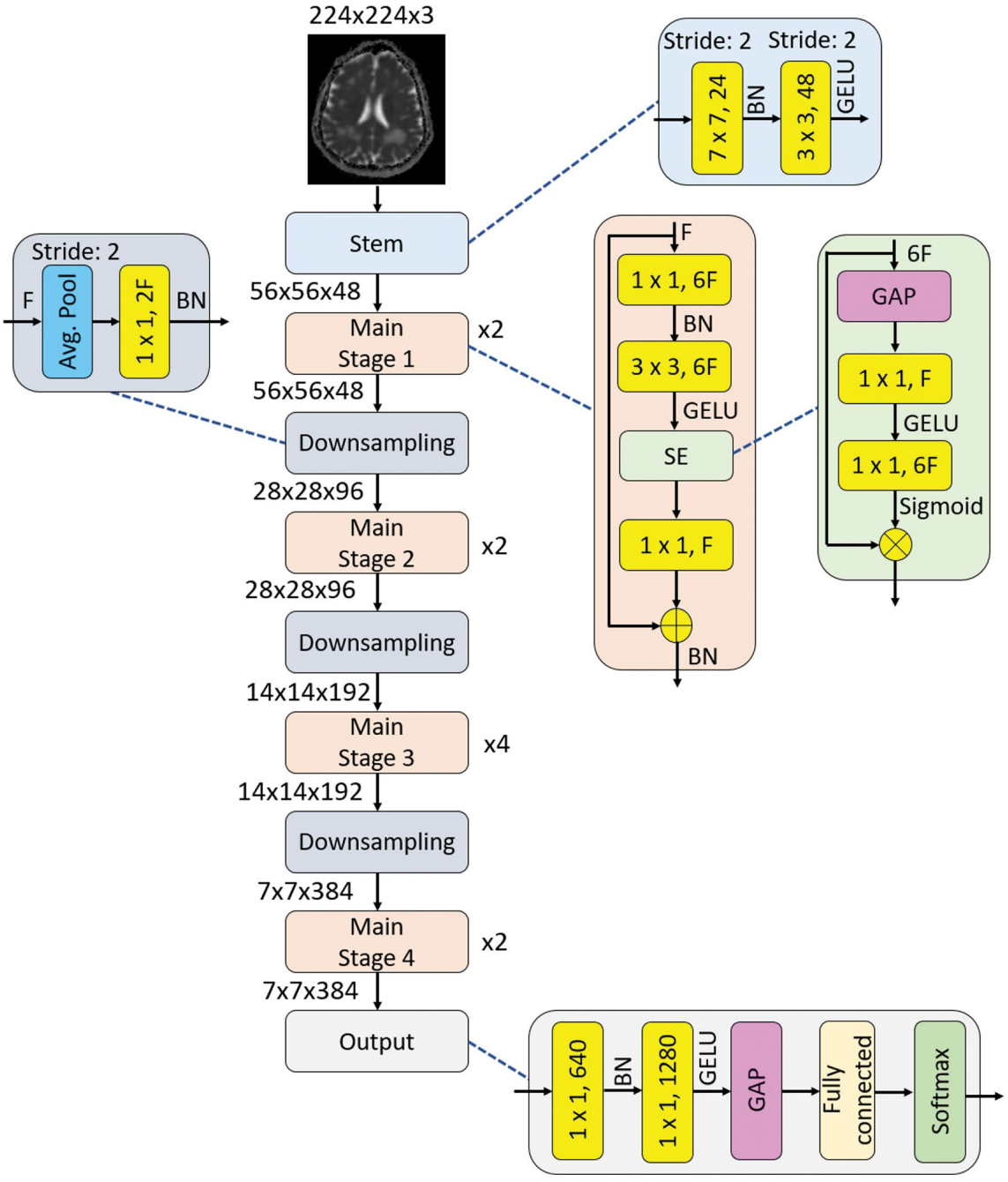

Fig. 2 Overview of the presented StrokeNeXt CNN model

The steps of the proposed StrokeNeXt-based DFE model are given below.

Step 1: Train the proposed StrokeNeXt by deploying training images.

Step 2: Create 49 patches deploying the following rule. The size of each patch is $56 \times 56 \times 3$, and stride is 28.

Step 3: By deploying GAP layer of the pretrained StrokeNeXt, we have generated features from the raw image and the generated feature patches.

$$f_1 = StrokeNeXt\left(Im, GAP\right) \tag{3}$$

$$f_{t+1} = StrokeNeXt\left(P_t, GAP\right), t \in \{1, 2, \ldots, 49\} \tag{4}$$

Herein, f the generated individual feature vector with a length of 1280, P: fixed-size patch with a size of $56 \times 56 \times 3$.

Step 4: Concatenate the generated feature vectors.

$$X\left(j + 1280 \times (a-1)\right) = f_t\left(j\right), \; a \in \{1, 2, \ldots, 50\} \tag{5}$$

Table 2 The mathematical details of the presented StrokeNeXt

Layer	Input	Operation	Output
Stem	224×224×3	7×7, 24, BN + GELU, stride: 2 3×3, 48, BN + GELU, stride: 2	56×56×48
Main 1	56×56×48	$\begin{bmatrix} 1\times1, 288 \\ 3\times3, 288 \\ SE, \frac{1}{6} \\ 1\times1, 48 \end{bmatrix} \times 2$	56×56×48
Downsampling 1	56×56×48	Average pooling with a filter size 2×2 and stride: 2, 1×1, 96, BN + GELU	28×28×96
Main 2	28×28×96	$\begin{bmatrix} 1\times1, 576 \\ 3\times3, 576 \\ SE, \frac{1}{6} \\ 1\times1, 96 \end{bmatrix} \times 2$	28×28×96
Downsampling 2	28×28×96	Average pooling with a filter size 2×2 and stride: 2, 1×1, 192, BN + GELU	14×14×192
Main 3	14×14×192	$\begin{bmatrix} 1\times1, 1152 \\ 3\times3, 1152 \\ SE, \frac{1}{6} \\ 1\times1, 192 \end{bmatrix} \times 4$	14×14×192
Downsampling 3	14×14×192	Average pooling with a filter size 2×2 and stride: 2, 1×1, 384, BN + GELU	7×7×384
Main 4	7×7×384	$\begin{bmatrix} 1\times1, 2304 \\ 3\times3, 2304 \\ SE, \frac{1}{6} \\ 1\times1, 384 \end{bmatrix} \times 2$	7×7×384
Output size	7×7×384	1×1, 640, BN, 1×1, 1280, GELU, GAP, fully connected layer, Softmax, classification	Number of classes
Total learnable parameters for 1000 classes			7.3 Million

Herein, X : the merged feature vector with a length of 64,000 (=1280 × 50).

Step 5: Apply the INCA feature selector to choose the best feature vector. The INCA is the developed version of the NCA feature selector. The parameters of the used INCA are given as follows. The range of iterations is from 100 to 1000. Therefore, 901 (=1000 – 100 + 1) feature vectors have been generated. In the loss value calculation, we have used the kNN classifier. The mathematical definition of the INCA feature selector has been defined below.

$$ix = NCA\left(X, y\right) \tag{6}$$

$$s^r\left(d,j\right) = X\left(d, ix\left(j\right)\right),\ d \in \{1,2,\ldots,Dim\},\ r \in \{1,2,\ldots,901\},\ j \in \{1,2,\ldots,r+99\} \tag{7}$$

$$loss\left(r\right) = \rho\left(s^r, y\right) \tag{8}$$

$$\left[mini, id\right] = \min\left(loss\right) \tag{9}$$

$$fetsel = s^{id} \tag{10}$$

Where ix: the qualified index, s: selected feature vector, y: actual outcome, Dim: the number of images, $\rho\left(.,.\right)$: loss ($loss$) value calculation, $mini$: minimum value, id: index of the minimum loss and $fetsel$: selected final features.

Using the INCA selector, we eliminated redundant features and retained only the most informative ones. INCA self-organizes by evaluating each feature subset with a classifier and selecting the subset that delivers the best classification performance. Reducing the feature space lowers model variance and the risk of overfitting. It also clarifies data geometry by removing irrelevant dimensions. This process sharpens class clusters and increases the decision-boundary margin. A larger margin improves generalization to new data and ensures stable performance under varying conditions.

Step 6: Classify the selected features deploying tkNN classifier. The mathematical definition of the tkNN classifier is illustrated below.

In the first step of tkNN classifier, the outputs have been generated employing iterative consecutive paramaters changing using a parameter bag. The parameter-based outcome generation's mathematical definition has been presented below.

$$pt_r = kNN\left(fetsel, y, PB\right), r \in \{1,2,\ldots,n_{par}\} \tag{11}$$

Herein, pt: paramater-based outcome, $kNN\left(.\right)$: kNN classifier, PB: parameters bag and n_{par}: number of parameters.

In the second step of the tkNN classifier, iterative majority voting has been applied to create voted outcomes.

$$vt_h = IMV\left(pt\right), h \in \{1,2,\ldots,n_{par}-2\} \tag{12}$$

where vt: voted outcome, $IMV\left(.\right)$: IMV function. The mathematical explaination of the IMV algorithm is illustrated below. Firstly, the classification accuracies of the

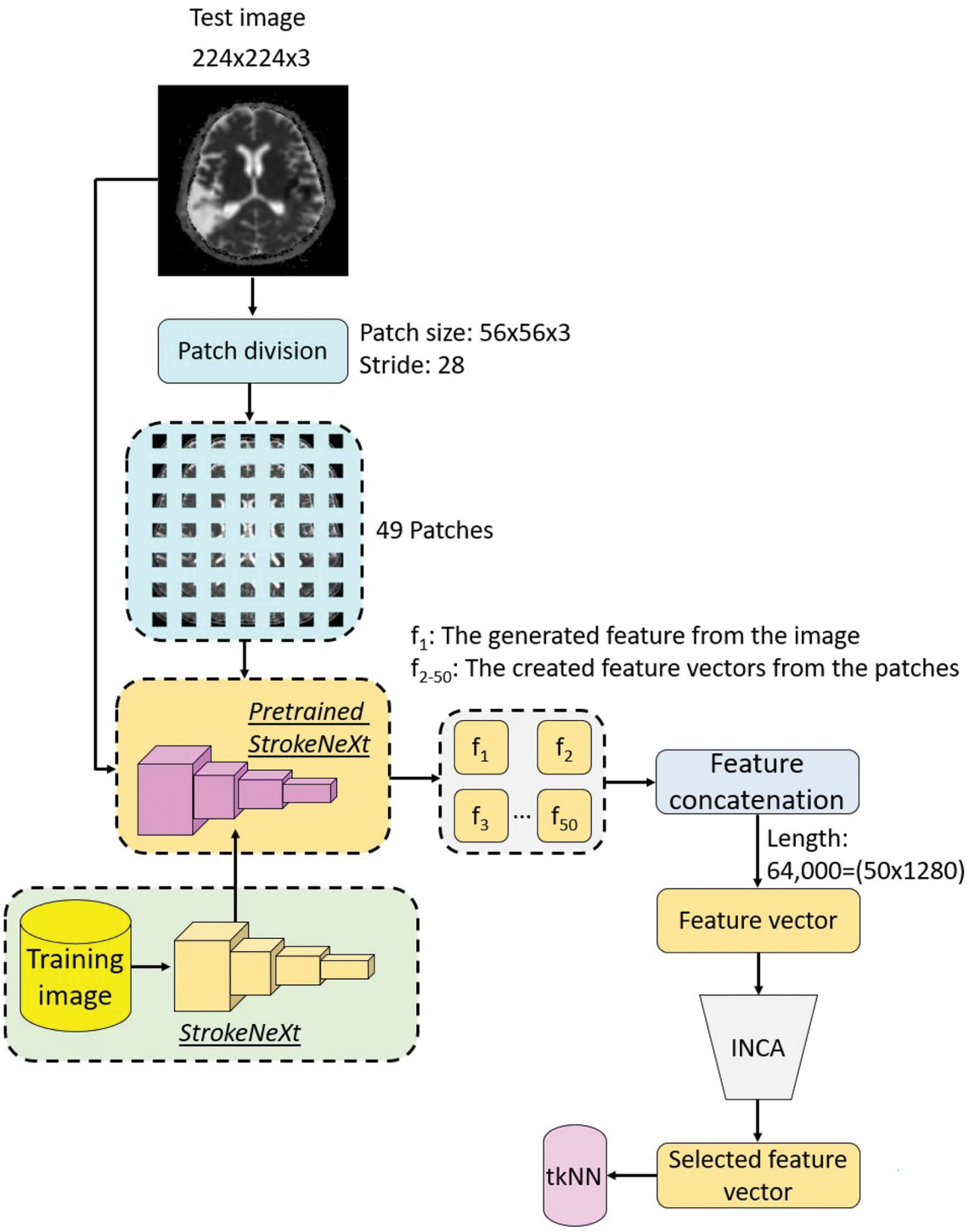

Fig. 3 The schematic overview of the presented StrokeNeXt-based DFE model

parameter-based outcomes have been computed. Utilizing the computed classification accuracies, the outputs have been ordered by descending. Subsequently, iterative mode operator has been applied to create voted outcomes.

$$acc_r = \theta\left(pt_r, y\right) \tag{13}$$

$$in = \arg sort\left(-acc\right) \tag{14}$$

$$vt_h = \varpi\left(pt_{in(1)}, pt_{in(2)}, \ldots, pt_{in(w)}\right), w \in \{3, 4, \ldots, n_{par}\} \tag{15}$$

Here, acc: classification accuracy,$\theta\left(.\right)$: classification acu in: the qualified identities and $\varpi\left(.\right)$: mode operator.

Deploying IMV voted outcomes have been created.

The last step of the tkNN classifier is selection the best outcome by deploying greedy algorithm.

$$acc_{n_{par}+h} = \theta\left(vt_h, y\right) \tag{16}$$

$$id_{\max} = \arg\max\left(acc\right) \tag{17}$$

$$fot = \begin{cases} pt_{id_{\max}}, id_{\max} \leq n_{par} \\ vt_{id_{\max}-n_{par}}, id_{\max} > n_{par} \end{cases} \tag{18}$$

Herein, id_{max}: identity of the output with maximum classification accuracy and fot: final output.

The utilized parameters of the tkNN classifier has been given in Section 5.

Experimental results

In this section, we present the experimental results of the proposed StrokeNeXt and StrokeNeXt-based DFE model using the collected dataset. The classification outcomes for these models were obtained within the MATLAB (2023a) programming environment. StrokeNeXt was developed with MATLAB's Deep Network Designer, and the model was trained utilizing this tool. Subsequently, the trained StrokeNeXt model was saved as a.mat file, which served as the foundation for the StrokeNeXt-based DFE model. To facilitate feature extraction, an.m file was created. Additionally, the INCA feature selector was coded using an.m file, initially employing a k-nearest neighbors (kNN) classifier to generate loss values. For classification purposes, the MATLAB Classification Learner Toolbox was utilized, offering access to over 30 classifiers. According to the classification outcomes, the kNN classifier emerged as the most accurate. Therefore, we applied to t algorithm to kNN and tkNN classifier has been utilized as classifier of the recommended StrokeNeXt-based DFE framework. Also kNN classifier was utilized as loss value generation function of the INCA feature selection function.

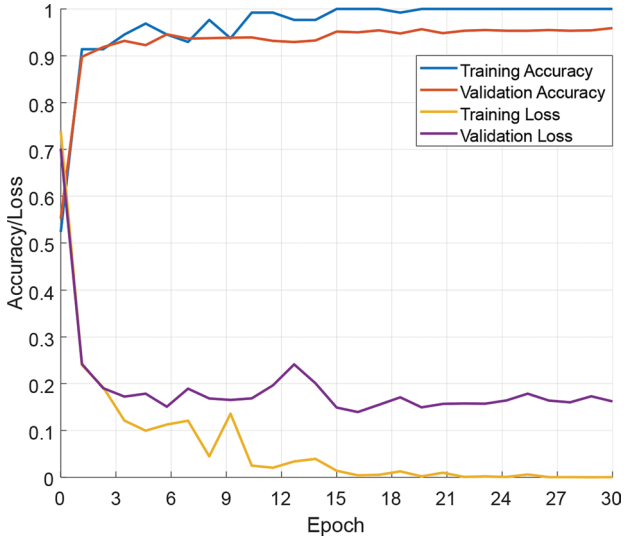

Fig. 4 Training and validation accuracies and loss values of the presented StrokeNeXt on the collected stroke CT and MR image dataset

The experimental settings for the proposed model are detailed as follows: The first model, StrokeNeXt, was trained using the following configurations: the solver was set to stochastic gradient descent with momentum (sgdm), the initial learning rate was 0.01, the maximum number of epochs was set to 30, L2 regularization was set at 0.0001, and the training and validation data were split in a 70:30 ratio. The training and validation curves of the proposed model are depicted in Fig. 4.

The proposed StrokeNeXt model achieved a final validation accuracy of 95.92% and a final validation loss of 0.1588. Additionally, the model reached 100% training accuracy and a training loss of 0. In Fig. 4, a vertical line at epoch 21 should highlight the optimal training duration. The x-axis label should read "Epoch Number" and the y-axis label should read "Accuracy/Loss." The legend should appear inside the plot area to improve readability. The region where training accuracy rises but validation accuracy stalls should be shaded to mark the onset of overfitting and show where further training yields little benefit.

For the development of the proposed Deep Feature Engineering (DFE) model, the settings utilized are as follows:

Feature extraction:

Patch size: $56 \times 56 \times 3$,

Stride: 28,

Number of patches: 49,

Feature extraction function: The GAP layer of the pretrained StrokeNeXt generates 1024 features from each input.

Feature generation: Feature extraction from 49 patches and a raw image. Therefore, the length of final feature vector is 64,000

Feature selection with INCA:

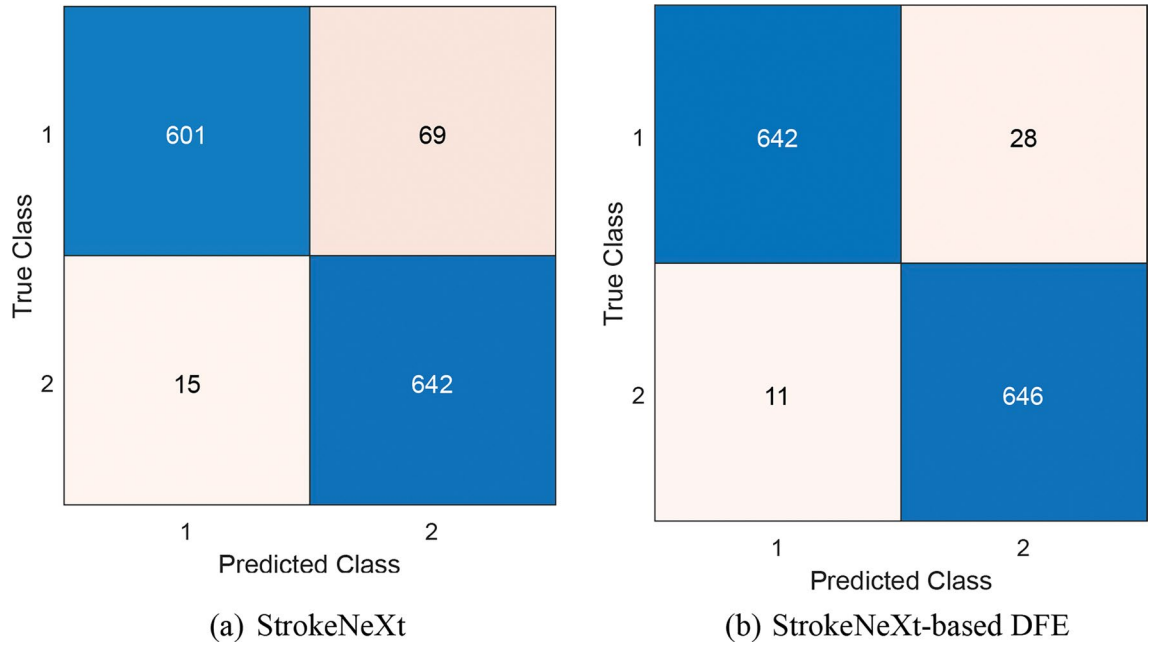

Fig. 5 Test confusion matrices of the proposed models. Herein, 1: Stroke and 2: Control classes. **a** StrokeNeXt. **b** StrokeNeXt-based DFE

Range of iteration: [100,1000],
Number of selected feature vector: 901,
Loss value generator: kNN classifier,
Final selected feature selection method: Selected feature vector with minimum loss value.
Number of selected feature vectors: 512
Classification with tkNN:
Parameters:
k values = from 1 to 10,
Weightining = Squared Inverse and Equal,
Distance: Cosine, City Block, Euclidean,
Number of parameter-based outcomes: 60,
Voted outcome generation function: IMV,
Number of voted outcomes: 58,
Number of total outcomes: 118,
Final outcome selection criteria: Maximum classification accuracy,
Validation: 10-fold CV.

To evaluate the performance of the proposed model, test classification results were analyzed using various metrics, including classification accuracy, precision, sensitivity, specificity, geometric mean, F1-score and Matthews Correlation Coefficient (MCC) [38]. The computed confusion matrices, demonstrating these results, are presented in Fig. 5.

Figure 5 shows that StrokeNeXt correctly identified 601 of 670 stroke cases and 642 of 657 control cases. It misclassified 69 strokes as controls and 15 controls as strokes. Figure 5b shows that the DFE model improved these results, correctly detecting 642 strokes and 646 controls while reducing misclassifications to 28 strokes and 11 controls. The reduction in both false negatives and false positives showcases that the DFE model has higher sensitivity and specificity than StrokeNeXt alone. This result confirms its stronger performance on the test set. Moreover, we apply statistical tests to show the differences of these both models. The McNemar test checked 1,327 observations (test images) where both models made a prediction. They disagreed on 55 of them. The new DFE model fixed 50 mistakes that StrokeNeXt made, while StrokeNeXt fixed only 5 mistakes made by the DFE. This big gap ($\chi^2 = 35.20$, $p \approx 2.1 \times 10^{-10}$, herein, $p \ll 0.01$) means the improvement is not due to chance. In plain numbers, the DFE lifts overall accuracy by about 3.4% (95% confidence: 2.3%–4.5%). It cuts false-negative cases from 69 to 28 and false-positive cases from 15 to 11. The DFE clearly performs better than the original StrokeNeXt model.

Table 3 The computed test results (%) of the presented models

Performance metric	StrokeNeXt	DFE model
Accuracy	93.67	97.06
Precision	97.56	98.32
Sensitivity	89.70	95.82
Specificity	97.72	98.33
Geometric mean	93.62	97.07
F1-score	93.47	97.05
MCC	87.64	94.15

Utilizing the confusion matrices depicted in Fig. 5, we have calculated six performance metrics summarized in Table 3.

According to Table 3, the proposed StrokeNeXt-based Deep Feature Engineering (DFE) model improved the test

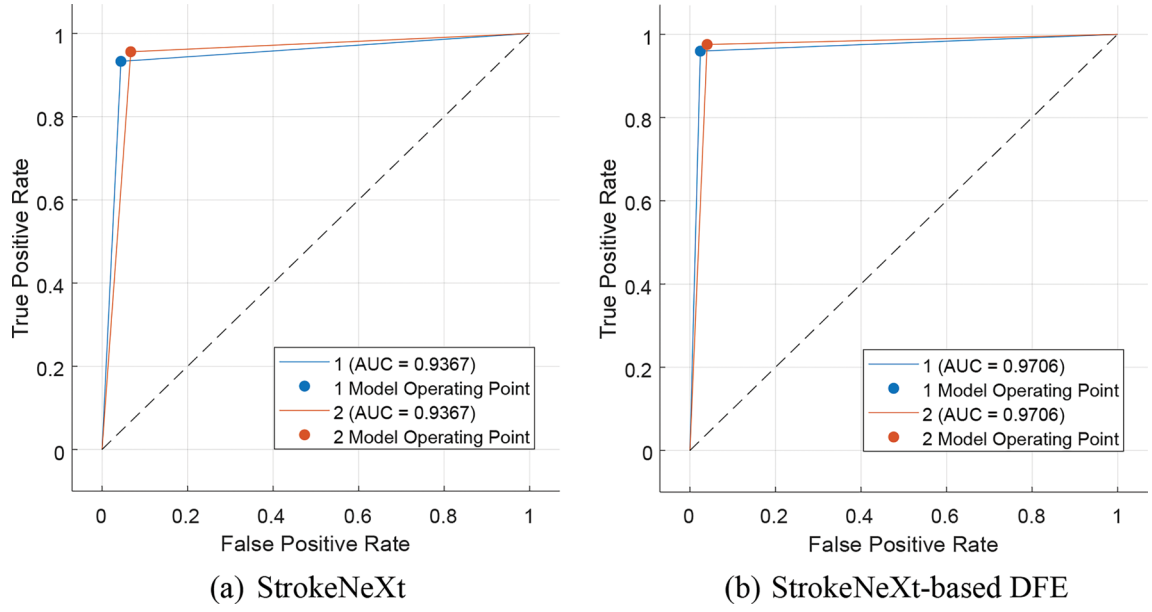

Fig. 6 The computed ROC curves. **a** StrokeNeXt. **b** StrokeNeXt-based DFE

classification accuracy by 3.39% (from 93.67% to 97.06%). Additionally, the DFE model outperformed the original StrokeNeXt across all performance metrics, indicating superior classification performance. Alsoi, Moreover, we have computed Receiver Operating Characteristic (ROC) for these results and the computed ROC curves have been illustrated in Fig. 6.

These ROC curves have been demonstrated that area under curve values (AUC) have been computed as 93.67% and 97.06% for StrokeNeXt and StrokeNeXt-based DFE consecutively.

These findings unequivocally show that the models presented are effective for stroke detection. Furthermore, with approximately 7.3 million learnable parameters, the proposed StrokeNeXt model is considered a lightweight CNN, highlighting its efficiency.

We measured StrokeNeXt's inference time on our system. Processing a $224 \times 224 \times 3$ image took approximately 10 ms. At this rate, StrokeNeXt can process about 100 images per second by using a simple graphical processing unit.

Discussions

Overview

In this research, we compiled a novel dataset of CT and MR images for stroke detection. CT imaging, which is more cost-effective than MRI, is frequently used in emergency services for stroke detection. We included CT images in our dataset to ensure our model's applicability in real-world scenarios. However, recognizing that some strokes are not visible in CT images, we also incorporated MR images to capture a wider range of stroke manifestations, thus creating a multimodal stroke image dataset.

Our secondary goal was to detect stroke with high classification performance while utilizing fewer learnable parameters. To achieve this, we introduced a new lightweight CNN model named StrokeNeXt. This model incorporates a modified ConvNeXt block with an SE block and leverages the MobileNetV2 architecture to achieve high classification performance with reduced parameter count. As a result, the total learnable parameters of StrokeNeXt were approximately 7.3 million. StrokeNeXt achieved a validation accuracy of 95.92% and a test accuracy of 93.67%. To further increase test classification performance and demonstrate the transfer learning capability of StrokeNeXt, we introduced a DFE model. This model employs fixed-size patches similar to the ViT and utilizes the INCA feature selector for optimal feature combination selection, selecting 512 out of 64,000 generated features. INCA examines 901 feature subsets across 100–1000 iterations. It computes a loss score for each subset using kNN. It then selects the subset with the lowest loss and cuts the feature count from 64,000 to 512. This reduction lowers memory use and speeds classification. The resulting 512 features raised test accuracy from 93.67% to 97.06%, improved generalization and showed less overfitting.

Comparisons

Consequently, our DFE model achieved a test classification accuracy of 97.06%. The DFE model employed an SVM classifier, which was identified as the most accurate shallow classifier within the MATLAB classification learner toolkit. To highlight the superiority of the tkNN classifier used, we compared it against other high-accuracy classifiers including Decision Tree (DT) [39],

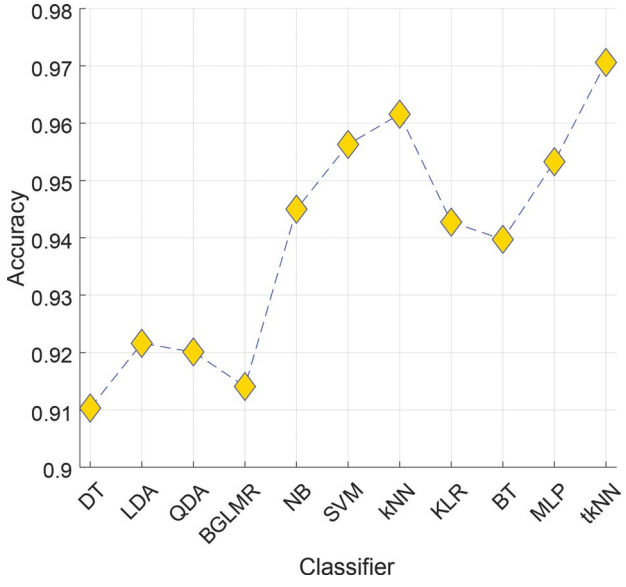

Fig. 7 Comparisons of the classifiers

Linear Discriminant Analysis (LDA) [40], Quadratic Discriminant Analysis (QDA) [41], Binary Generalized Linear Model Logistic Regression (BGLMLR) [42], Naïve Bayes (NB) [43], SVM [44, 45], kNN [46], Bagged Tree (BT) [47], Multilayer Perceptron (MLP) [48], and Kernel Logistic Regression (KLR) [49], with results depicted in Fig. 7.

According to Fig. 7, the tkNN classifier attained the best classification accuracy among the utilized 11 classifiers. Figure 7 presents the test accuracies of 11 classifiers on the StrokeNeXt–INCA feature set. The DT reached 91.03%, LDA 92.16%, QDA 92.01%, and BGLMR 91.41%. NB achieved 94.50%, SVM 95.63%, and kNN 96.16%. KLR scored 94.27%, Bagged Tree 93.97%, and MLP 95.33%. The highest accuracy belongs to tkNN at 97.06%. kNN stands out as the best standard shallow model with 96.16%, while SVM and MLP also exceed 95%. The lowest performance appears with DT at 91.03%. These results confirm the strength of the StrokeNeXt–INCA features and the added value of the tkNN ensemble. The best of the used shallow classifier (other classifiers) is the kNN algorithm. Thus, we applied to t algorithm to kNN and we have obtained tkNN classifier to increase the classification performance. kNN classifier attained 96.16% classification accuracy while tkNN classifier reached 97.06% classification accuracy on the utilized dataset. In this aspect, tkNN classifier increased 0.90% point of the kNN classifier. These results unequivocally demonstrate the effectiveness of the feature vectors generated by the proposed StrokeNeXt and INCA.

We have included these results in Table 4 for a detailed analysis to present comparative outcomes.

Our model achieved satisfactory test performance based on the comparative results, underscoring our introduction of a new CNN designed for stroke detection using a multimodal image dataset. These findings indicate that our model can detect strokes in CT and MR images. Moreover, the utilized architecture is a fully convolutional lightweight architecture and we have increased the classification performance by deploying the recommended DFE model. Inthis aspect, we have contributed to:

Table 4 Comparative results

Study	Method	Data	Data augmentation	The accuracy (%)
Chin et al. [50]	CNN	256 (128 train, 128 test)	Yes	92.97
Gahiwad et al. [51]	CNN	2551 (60:40)	No	90.00
Tursynova et al. [52]	CNN	610 (80:20)	Yes	81.00
Gautam and Raman [53]	CNN	120 (80:20)	No	93.33
Raghavendra et al. [54]	Nonlinear feature extraction	1603 (10-fold CV)	No	97.37
Korra et al. [55]	U-Net	2501 (unspecified)	Yes	94.57
UmaMaheswaran et al. [56]	Feature engineering	2501 (unspecified)	No	97.00
Saleem et al. [57]	Genetic algorithm, bidirectional long short-term memory	1900 (10-fold CV)	No	96.50
Acharya et al. [58]	HOS features	267	No	97.60
Tursynova et al. [59]	CNN	993 (80:20)	Yes	72.28
UmaMaheswaran et al. [56]	Local binary pattern, Gabor, Discrete wavelet transform	2501 (unspecified)	No	97.00
Chen et al. [60]	CNN	96 (unspecified)	No	95.83
Boriesosdick et al. [61]	DL-based LVO	443 (unspecified)	No	87.6
Ahmed et al. [62]	3D CNN	2501 (70:30)	Yes	92.5
Beevi M et al. [63]	Bayesian CNN	10532 (8425:2107)	Yes	92.88
Moldovanu et. al [38]	Custom CNN	5336 (4009 train, 1327 test)	No	80.03
	Hybrid DFE model			93.14
Our study	StrokeNeXt	5336 (4009 train, 1327 test)	No	93.67
	DFE model			97.06

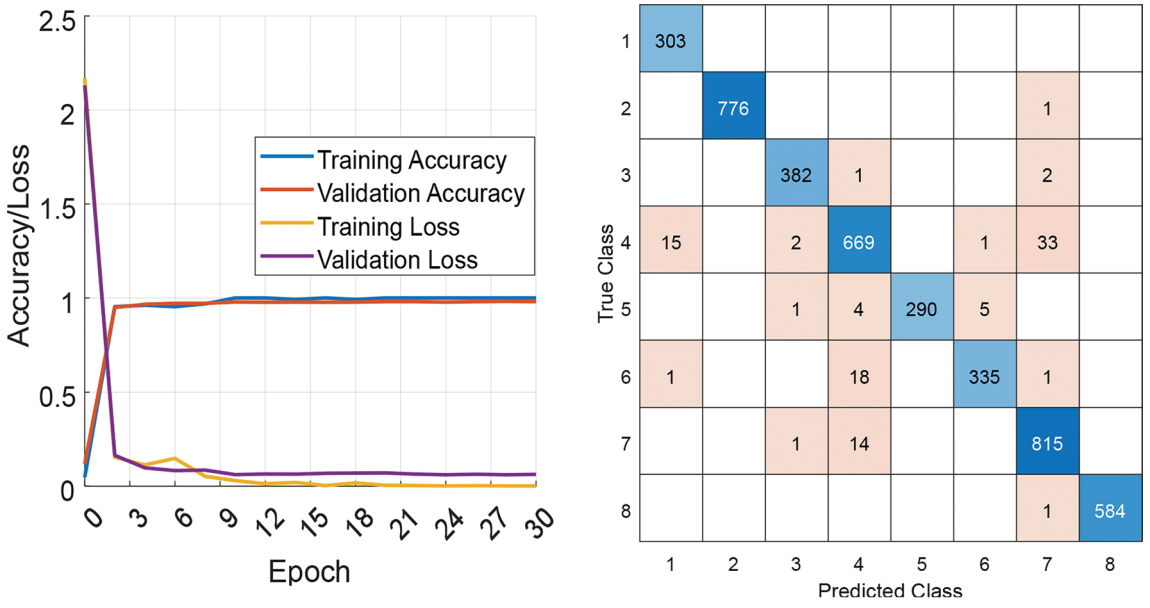

(a) Training and validation accuracy and loss over epochs

(b) Confusion matrix on the test set.

Fig. 8 Application of the presented StrokeNeXt to the blood cell image dataset. **a** Training and validation accuracy and loss over epochs. **b** Confusion matrix on the test set

Table 5 The results of the presented StrokeNeXt on the blood cell image dataset

Performance metric	Value
Training accuracy	100%
Training loss	3.5835e-04
Validation accuracy	98.25%
Validation loss	0.0542
Test accuracy	97.63%

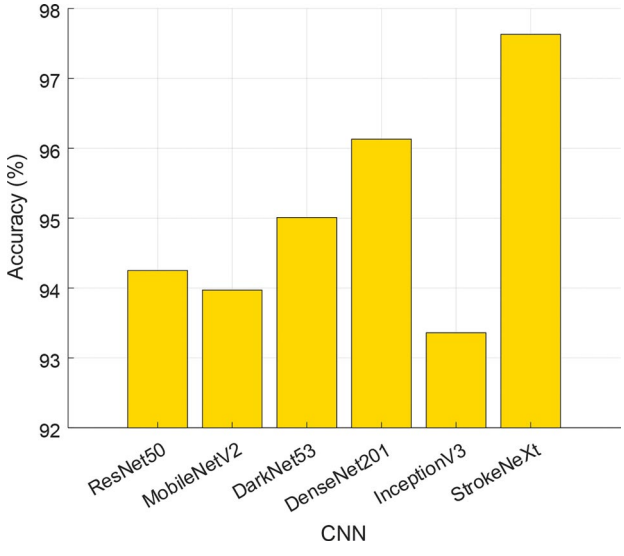

Fig. 9 Comparative test accuracies on the blood cell dataset

- New generation CNN architecture development,
- Lightweight deep learning development research area,
- Feature engineering with deep learning models (DFE),
- By applying StrokeNeXt and StrokeNeXt-based DFE on the curated multimodal stroke dataset, this research contributes to automatic stroke detection.

Test of additional dataset

To assess the general classification performance of StrokeNeXt, we applied it to a publicly available blood cell image dataset [64, 65]. This dataset contains 17 092 microscopic peripheral blood cell images across eight classes: (1) basophils, (2) eosinophils, (3) erythroblasts, (4) immature granulocytes, (5) lymphocytes, (6) monocytes, (7) neutrophils, and (8) platelets. eWe used 12,837 images for training and 4,255 images for testing. We trained StrokeNeXt under the same settings as the stroke dataset. The resulting training and validation curves and the test confusion matrix appear in Fig. 8.

Per Fig. 8, the computed results have been tabulated in Table 5.

We then compared StrokeNeXt to five standard CNNs—ResNet50, MobileNetV2, DarkNet53, DenseNet201, and InceptionV3—using the same data split and training protocol. The comparative test accuracies are illustrated in Fig. 9.

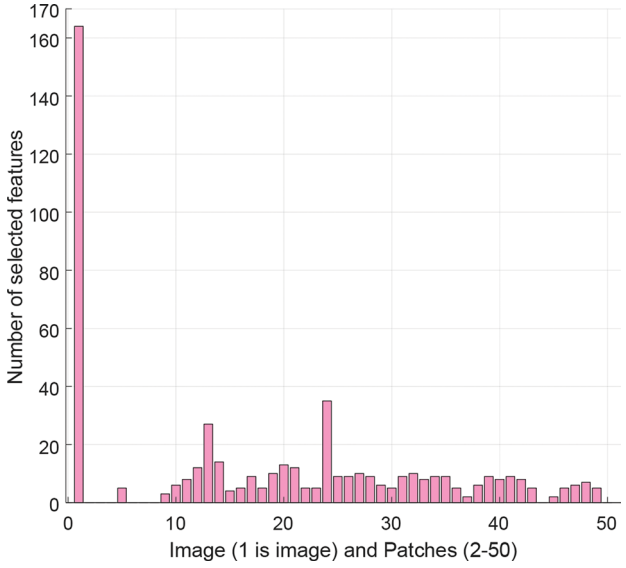

Fig. 10 Generation of the selected features

In Fig. 9, ResNet50 achieved 94.25% test accuracy, MobileNetV2 93.97%, DarkNet53 95.01%, DenseNet201 96.13%, and InceptionV3 93.36%. StrokeNeXt outperformed all five models with 97.63% accuracy. These results illustrate that the presented StrokeNeXt's strong generalization ability and its effectiveness across diverse biomedical imaging tasks.

Feature analysis and interpretable results

We further analyzed the features selected by the INCA feature selector, which chose 512 features from the generated pool of 64,000 features. The origins of these selected features are illustrated in Fig. 10, providing insights into the contributions of the entire image and the individual patches to the classification process.

According to Fig. 10, 164 selected 512 features were generated from the whole image, while the remaining 348 were derived from patches. This demonstrates that the patch-based feature extraction significantly contributes to achieving a 97.06% test classification accuracy. Furthermore, these results are illustrated with a sample image in Fig. 11 to provide explainable insights.

According to Fig. 11, our model identifies and generates features from regions of interest, effectively highlighting its capability. This figure convincingly shows that the proposed StrokeNeXt operates as an interpretable model, intelligently focusing on relevant areas for feature extraction.

Also, by utilizing Gradient-weighted Class Activation Mapping (Grad-CAM) [66], heatmaps were generated. The computed heatmaps for sample images are illustrated in Fig. 12.

Figure 12a and c display a CT slice and an MR slice, respectively. Figure 12c and d overlay Grad-CAM activations on the original images. In these heatmaps, red and yellow regions denote areas of highest model attention, while green and blue regions carry lower weight. In Fig. 12b, the heatmap peaks over the hyper dense region in the left parietal lobe, matching the acute hemorrhage. In Fig. 12d, the activation concentrates on the periventricular hyper intensity in the MR scan corresponding to the ischemic lesion. Cooler zones correspond/illustrate to healthy tissue. These overlays confirm that StrokeNeXt directs its decisions to clinically relevant regions and lend interpretability to its predictions.

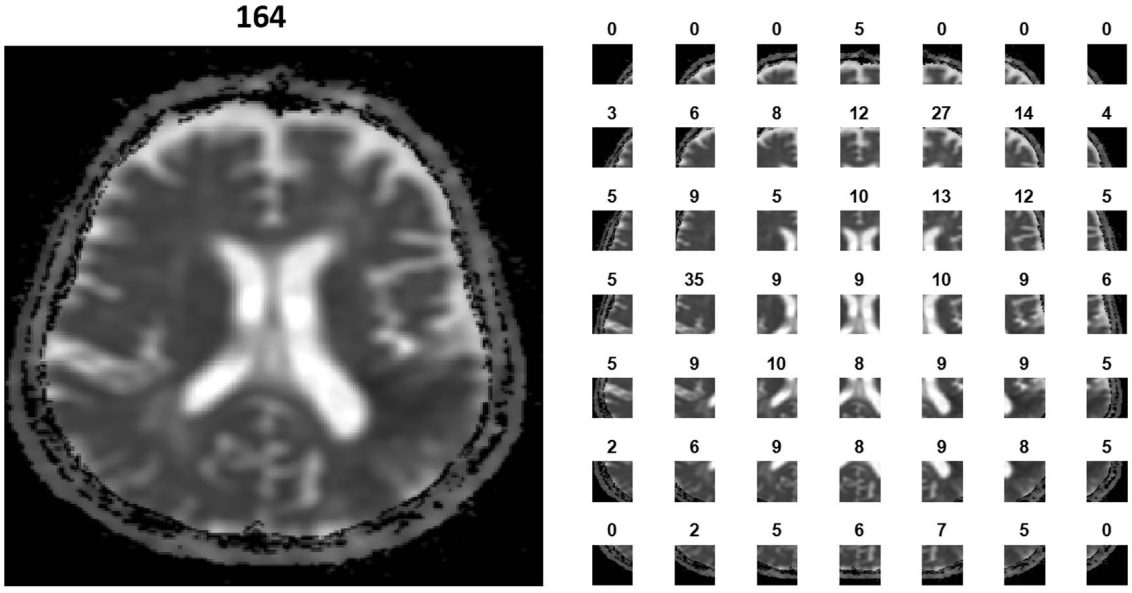

Fig. 11 The distribution of the selected feature per the used input using a sample image

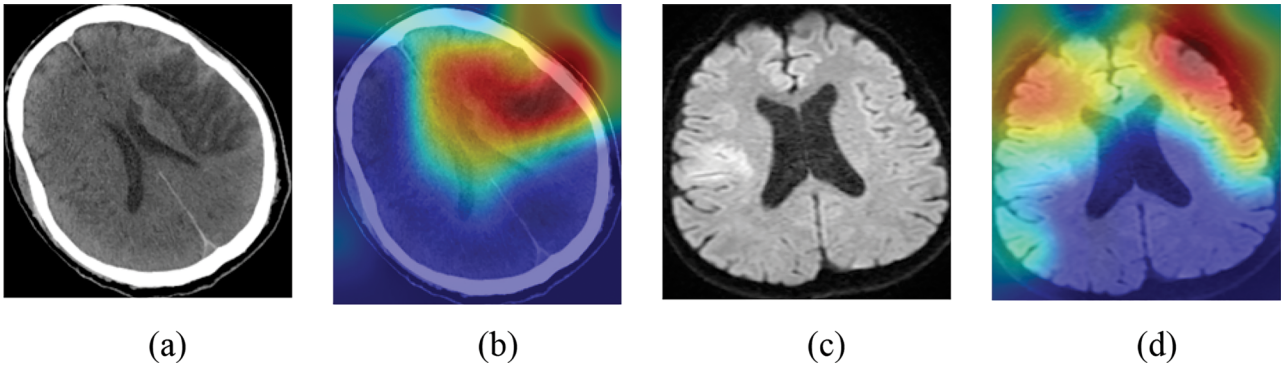

Fig. 12 Heatmaps of the CT and MR image samples. (**a**) CT image, (**b**) CT heatmap, (**c**) MR image, (**d**) MR heatmap

Highlights

Highlights of this research are explained below.

Findings and advantages:

- StrokeNeXt achieved 93.67% test accuracy and 95.92% validation accuracy. These results show the model's robustness and its ability to detect stroke features in the dataset.
- The introduced DFE approach raised test accuracy to 97.06%. This result shows the value of advanced feature extraction and selection methods such as patch-based extraction and the INCA selector to improve model predictions.
- StrokeNeXt handles a multimodal dataset of CT and MR images. This ability illustrates the model's versatility and its use in clinical settings with multiple imaging types.
- INCA feature selector chose many features from patch-based extractions that helped achieve high test accuracy (348 out of the 512 features were selected from patches). This result shows the value of focus on local image areas for feature creation.
- StrokeNeXt generates features from regions of interest, as shown in Fig. 7. This design lets the model focus on important image areas and match human visual patterns.
- StrokeNeXt has about 7.3 million parameters. This small size makes it a lightweight CNN that delivers high performance without heavy computation.
- StrokeNeXt architecture and methods allow scale to new datasets and imaging types. This flexibility lets StrokeNeXt adapt to advances in medical imaging and stroke research.
- Table 4 showcases comparative results that confirm StrokeNeXt's effectiveness in stroke detection. These results place StrokeNeXt above other models and support its use in clinical practice.
- StrokeNeXt achieved the highest accuracy on the public blood cell image dataset (see Fig. 11). It exceeded the performance of other CNNs and confirmed its strong generalization ability across biomedical imaging tasks.
- StrokeNeXt's accuracy, efficiency, and versatility showcase its use in clinical practice. StrokeNeXt can help doctors and medical professionals detect strokes quickly and accurately to speed decision-making and improve patient outcomes.

Limitations:

- The utilized dataset is a relatively bigger dataset. However, larger and more diverse datasets can be collected by collaborating more medical centers.
- The dataset lacks sufficient variety to fully assess StrokeNeXt's classification capabilities.

Future directions:

- The researchers can gather data from multiple medical centers and regions to expand the dataset and include varied imaging characteristics and stroke types.
- The dataset will cover different stroke subtypes, patient groups, and imaging modalities to improve classification accuracy across clinical scenarios.
- Long-term and prospective studies with StrokeNeXt can assess its performance in real-world settings and its impact on patient outcomes.
- Integration of StrokeNeXt into healthcare information systems and clinical workflows will address practical adoption challenges and support clinical use.
- We plan to integrate multi-head self-attention (MHSA) and patch embedding to the recommended StrokeNeXt to present second version of this CNN.
- In this research, we have presented a lightweight version of the recommended StrokeNeXt; lighter and bigger versions of this CNN can be presented by changing the number of filters and the number of repetitions.

- New CNN models based on StrokeNeXt will be developed and tested on large public image collections such as CIFAR and ImageNet.

Potential implications:

- StrokeNeXt enables real-time triage in emergency services. It flags suspected stroke cases on CT and MR scans and reduces door-to-needle time.
- In neuroradiology, the model serves as a first-read assistant. It can generate report by using XAI techniques to help doctors.
- Deployment in tele-stroke networks supports remote hospitals without on-site neuroradiologists. It improves access to timely stroke diagnosis and the mortality rate can be decreased.
- Integration with hospital PACS and electronic health records streamlines clinical workflows and embeds automated detection into routine imaging review.
- In low-resource settings, a lightweight version of StrokeNeXt runs on standard personal computers, workstations and expands diagnostic capacity where imaging expertise is limited.
- Aggregation of outputs from multiple centers informs public health surveillance and provides data on stroke incidence, subtypes, and outcomes across regions.
- As an educational tool, StrokeNeXt assists training for radiology and neurology residents by giving immediate feedback on image interpretation and common stroke patterns.
- StrokeNeXt features with clinical and laboratory data can be combined to create personalized prognosis models that guide treatment decisions and predict recovery.

Conclusions

In this research, we introduce an innovative CNN architecture termed StrokeNeXt. StrokeNeXt was tested on a multimodal stroke image dataset containing both CT and MR images. The model achieved 93.67% test accuracy. To increase this accuracy, we developed a StrokeNeXt-based DFE model, which yielded 97.06% test accuracy. These results confirm the model's strong ability to detect stroke patterns in complex image sets.

StrokeNeXt performs equally well on CT and MRI scans. This consistency provides reliable performance in hospitals with different imaging tools and supports stroke diagnosis across clinical settings.

The introduced StrokeNeXt has about 7.3 million learnable parameters. This compact design ensures fast execution and requires minimal hardware. Hospitals can run StrokeNeXt on standard workstations without extra investment.

This research reduces diagnosis time and lowers radiologists' workload, as StrokeNeXt's test time is about 10 ms per image. Its high accuracy and speed may lead to faster treatment decisions and improved patient outcomes.

These findings establish a solid foundation for future work on CNN methods in stroke detection. StrokeNeXt offers a clear path for developing and adopting advanced, efficient diagnostic tools in clinical practice.

Acknowledgement
The authors have no acknowledgements to declare.

Author contributions
All authors contributed to the conceptualization, methodology, and supervision of the project. EE, FY, OB, EA, IS, AHB, SD, and TT contributed to the conceptualization, methodology, validation, formal analysis, investigation, resources, data curation, and visualization. SD, TT and EA led the software development and contributed to the writing, review and editing. TT provided supervision and project administration. EE, FY, OB, EA, IS, AHB, SD, and TT were involved in the original draft preparation and writing. SD and TT led the review and editing process. All authors have reviewed, edited, and approved the final version of the manuscript.

Funding
The authors declare that no funds, grants, or other support were received during the preparation of this manuscript.

Data availability
The datasets generated during and/or analysed during the current study are not openly available for reasons of patient confidentiality however anonymised data may be available from the corresponding author on reasonable request.

Declarations

Ethics approval and consent to participate
This research has been approved on ethical grounds by the Non-Invasive Ethics Committee, Ankara Provincial Health Directorate, Yildirim Beyazit University Yenimahalle Training and Research Hospital, on December 07, 2023 (E-2023-76). Individual informed consent was waived because this was a retrospective study. All methods were performed in accordance with the relevant guidelines and regulations.

Consent for publication
None.

Clinical trial number
Not applicable.

Competing interests
The authors have no relevant financial or non-financial interests to disclose.

Received: 28 January 2025 / Accepted: 11 May 2025
Published online: 05 June 2025

References

1. Miller EL, Murray L, Richards L, Zorowitz RD, Bakas T, Clark P, et al. Comprehensive overview of nursing and interdisciplinary rehabilitation care of the stroke patient: a scientific statement from the American Heart Association. Stroke. 2010;41:2402–48.
2. Meschia JF, Bushnell C, Boden-Albala B, Braun LT, Bravata DM, Chaturvedi S, et al. Guidelines for the primary prevention of stroke: a statement for healthcare professionals from the American Heart Association/American Stroke Association. Stroke. 2014;45:3754–832.

3. WHO. World Health Organization, Stroke, Cerebrovascular accident. 2024. https://www.emro.who.int/health-topics/stroke-cerebrovascular-accident/index.html. Accessed 20 Dec 2024.
4. Labarthe DR. Epidemiology and prevention of cardiovascular diseases: a global challenge: a global challenge. 2010.
5. Sabayan B. Primary prevention of ischemic stroke. In: Seminars in neurology, vol 42. New York, NY: Thieme Medical Publishers, Inc.; 2022. pp. 571–82.
6. Inamdar MA, Raghavendra U, Gudigar A, Chakole Y, Hegde A, Menon GR, et al. A review on computer aided diagnosis of acute brain stroke. Sensors. 2021;21:8507.
7. Jäger H. Diagnosis of stroke with advanced CT and MR imaging. Br Med Bul. 2000;56:318–33.
8. Haleem A, Javaid M, Singh RP, Suman R. Medical 4.0 technologies for healthcare: features, capabilities, and applications. Internet Things Cyber-Phys Syst. 2022;2:12–30.
9. Thompson RF, Valdes G, Fuller CD, Carpenter CM, Morin O, Aneja S, et al. Artificial intelligence in radiation oncology: a specialty-wide disruptive transformation? Radiother Oncol. 2018;129:421–26.
10. Dwivedi YK, Hughes L, Ismagilova E, Aarts G, Coombs C, Crick T, et al. Artificial Intelligence (AI): multidisciplinary perspectives on emerging challenges, opportunities, and agenda for research, practice and policy. Int J Inf Manage. 2021;57:101994.
11. Pedro F, Subosa M, Rivas A, Valverde P. Artificial intelligence in education: challenges and opportunities for sustainable development. Paris, France: UNESCO. 2019. https://unesdoc.unesco.org/ark:/48223/pf0000366994?posInSet=1&queryId=2c58492c-931f-47d2-967d-7194427f4062. Accessed 20 Dec 2024.
12. Dosovitskiy A, Beyer L, Kolesnikov A, Weissenborn D, Zhai X, Unterthiner T, et al. An image is worth 16×16 words: transformers for image recognition at scale. arXiv preprint arXiv:201011929. 2020.
13. Atteia G, El-kenawy E-SM, Samee NA, Jamjoom MM, Ibrahim A, Abdelhamid AA, et al. Adaptive dynamic dipper throated optimization for feature selection in medical data. Comput Mater Continua. 2023;75:1883–900.
14. Gaber KS, Singla M,K. Predictive analysis of groundwater resources using random forest regression. J Artif Intell Metaheuristics (JAIM). 2025;9:11–19.
15. Mohamed ME. A review on waste management techniques for sustainable. Energy Production Metaheuristic Optimization Review (MOR). 2025;3:47–58.
16. Mishra P, Alhussan AA, Khafaga DS, Lal P, Ray S, Abotaleb M, et al. Forecasting production of potato for a sustainable future: global market analysis. Potato Res. 2024;67:1671–90.
17. El-Kenawy E-SM, Khodadadi N, Mirjalili S, Abdelhamid AA, Eid MM, Ibrahim A. Greylag goose optimization: nature-inspired optimization algorithm. Expert Syst Appl. 2024;238:122147.
18. Subudhi A, Acharya UR, Dash M, Jena S, Sabut S. Automated approach for detection of ischemic stroke using Delaunay Triangulation in brain MRI images. Comput Biol Med 2018;103:116–29.
19. Sudharani K, Sarma T, Prasad KS. Brain stroke detection using k-nearest neighbor and minimum mean distance technique. 2015 International Conference on Control, Instrumentation, Communication and Computational Technologies (ICCICCT): IEEE; 2015. p. 770–76.
20. Cetinoglu YK, Koska IO, Uluc ME, Gelal MF. Detection and vascular territorial classification of stroke on diffusion-weighted MRI by deep learning. Eur. J. Radiol. 2021;145:110050.
21. Aishvarya R, Anand R, Vasundhara B, Sudha DS. Early detection of brain stroke using MRI images. Int Res J Eng Technol. 2020;7:2258–61.
22. F-h T, Ng DK, Chow DH. An image feature approach for computer-aided detection of ischemic stroke. Comput Biol Med. 2011;41:529–36.
23. Badriyah T, Sakinah N, Syarif I, Syarif DR. Machine learning algorithm for stroke disease classification. 2020 International Conference on Electrical, Communication, and Computer Engineering (ICECCE): IEEE; 2020. p. 1–5.
24. Krishna V, Kiran JS, Rao PP, Babu GC, Babu GJ. Early detection of brain stroke using machine learning techniques. 2021 2nd International Conference on Smart Electronics and Communication (ICOSEC): IEEE; 2021. p. 1489–95.
25. Ayoub M, Liao Z, Hussain S, Li L, Zhang CW, Wong KK. End to end vision transformer architecture for brain stroke assessment based on multi-slice classification and localization using computed tomography. Computerized Med Imaging Graphics. 2023;109:102294.
26. Gautam A, Raman B. Brain strokes classification by extracting quantum information from CT scans. Multimedia Tools Appl. 2023;82:15927–43.
27. Lee K-Y, Liu -C-C, Chen DY-T, Weng C-L, Chiu H-W, Chiang C-H. Automatic detection and vascular territory classification of hyperacute staged ischemic stroke on diffusion weighted image using convolutional neural networks. Sci Rep. 2023;13:404.
28. Patel CH, Undaviya D, Dave H, Degadwala S, Vyas D. EfficientNetB0 for brain stroke classification on computed tomography scan. 2023 2nd International Conference on Applied Artificial Intelligence and Computing (ICAAIC): IEEE; 2023. p. 713–18.
29. Dogan S, Baygin M, Tasci B, Loh HW, Barua PD, Tuncer T, et al. Primate brain pattern-based automated Alzheimer's disease detection model using EEG signals. Cogn Neurodyn. 2023;17:647–59.
30. Liu Z, Lin Y, Cao Y, Hu H, Wei Y, Zhang Z, et al. Swin transformer: hierarchical vision transformer using shifted windows. Proceedings of the IEEE/CVF international conference on computer vision2021. p. 10012–22.
31. Liu Z, Mao H, Wu C-Y, Feichtenhofer C, Darrell T, Xie S. A convnet for the 2020s. Proceedings of the IEEE/CVF conference on computer vision and pattern recognition2022. p. 11976–86.
32. Nguyen E, Poli M, Faizi M, Thomas A, Wornow M, Birch-Sykes C, et al. Hyenadna: long-range genomic sequence modeling at single nucleotide resolution. Adv Neural Inf Process Syst. 2024;36:43177–201.
33. Zheng A, Casari A. Feature engineering for machine learning: principles and techniques for data scientists: "OReilly Media, Inc." 2018.
34. Sengupta S, Basak S, Saikia P, Paul S, Tsalavoutis V, Atiah F, et al. A review of deep learning with special emphasis on architectures, applications and recent trends. Knowl-Based Syst. 2020;194:105596.
35. Wang S, Huang L, Gao A, Ge J, Zhang T, Feng H, et al. Machine/deep learning for software engineering: a systematic literature review. IEEE Trans Softw Eng. 2022;49:1188–231.
36. Xue B, Zhang M, Browne WN, Yao X. A survey on evolutionary computation approaches to feature selection. IEEE Trans Evol Comput. 2015;20:606–26.
37. Tuncer T, Dogan S, Özyurt F, Belhaouari SB, Bensmail H. Novel multi center and threshold ternary pattern based method for disease detection method using voice. IEEE Access. 2020;8:84532–40.
38. Moldovanu S, Tăbăcaru G, Barbu M. Convolutional neural network–machine learning model: hybrid model for meningioma tumour and healthy brain classification. J Imaging. 2024;10:235.
39. Safavian SR, Landgrebe D. A survey of decision tree classifier methodology. IEEE Trans Syst Man Cybern Syst. 1991;21:660–74.
40. Zhang Y, Zhou X, Witt RM, Sabatini BL, Adjeroh D, Wong ST. Dendritic spine detection using curvilinear structure detector and LDA classifier. Neuroimage. 2007;36:346–60.
41. Bhattacharyya S, Khasnobish A, Chatterjee S, Konar A, Tibarewala D. Performance analysis of LDA, QDA and KNN algorithms in left-right limb movement classification from EEG data. 2010 International conference on systems in medicine and biology: IEEE; 2010. p. 126–31.
42. Deng Z, Kammoun A, Thrampoulidis C. A model of double descent for high-dimensional binary linear classification. Inf Inference J IMA. 2022;11:435–95.
43. Ng AY, Jordan MI. On discriminative vs. generative classifiers: a comparison of logistic regression and naive bayes. Adv Neural Inf Process Syst. 2001;14:841–48.
44. Vapnik V. The Support Vector Method of Function Estimation. Nonlinear Modeling: Springer; 1998. p. 55–85.
45. Vapnik V. The nature of statistical learning theory. Springer science & Business Media. New York, NY: Springer; 2013.
46. Maillo J, Ramírez S, Triguero I, Herrera F. kNN-IS: an Iterative Spark-based design of the k-Nearest Neighbors classifier for big data. Knowledge-Based Syst. 2017;117:3–15.
47. Biggio B, Corona I, Fumera G, Giacinto G, Roli F. Bagging classifiers for fighting poisoning attacks in adversarial classification tasks. Multiple Classifier Systems: 10th International Workshop, MCS 2011, Naples, Italy, June 15-17, 2011 Proceedings 10: Springer; 2011. p. 350–59.
48. Biswas SK, Mia MMA. Image reconstruction using multi layer perceptron (mlp) and support vector machine (svm) classifier and study of classification accuracy. Int J Sci Technol Res. 2015;4:226–31.
49. Zhu J, Hastie T. Kernel logistic regression and the import vector machine. J Comput Graph Stat. 2005;14:185–205.
50. Chin C-L, Lin B-J, Wu G-R, Weng T-C, Yang C-S, Su R-C, et al. An automated early ischemic stroke detection system using CNN deep learning algorithm. 2017 IEEE 8th International Conference on Awareness Science and Technology (iCAST): IEEE; 2017. p. 368–72.
51. Gahiwad P, Deshmane N, Karnakar S, Mali S, Pise R. Brain stroke detection using CNN algorithm. 2023 IEEE 8th International Conference for Convergence in Technology (I2CT): IEEE; 2023. p. 1–4.

52. Tursynova A, Omarov B, Tukenova N, Salgozha I, Khaaval O, Ramazanov R, et al. Deep learning-enabled brain stroke classification on computed tomography images. Comput Mater Continua. 2023;75:1431–46.
53. Gautam A, Raman B. Towards effective classification of brain hemorrhagic and ischemic stroke using CNN. Biomed Signal Process Control. 2021;63:102178.
54. Raghavendra U, Pham T-H, Gudigar A, Vidhya V, Rao BN, Sabut S, et al. Novel and accurate non-linear index for the automated detection of haemorrhagic brain stroke using CT images. Complex Intelligent Syst. 2021;7:929–40.
55. Korra S, Soora NR, Jahan T, Ramana N, Rajesh A. Brain CT image processing using U-net model with data augmentation for detection of ischemic and haemorrhage strokes. Int J Intell Syst and Appl Eng. 2024;12:72–82.
56. UmaMaheswaran S, Ahmad F, Hegde R, Alwakeel AM, Zahra SR. Enhanced non-contrast computed tomography images for early acute stroke detection using machine learning approach. Expert Syst Appl. 2024;240:122559.
57. Saleem MA, Javeed A, Akarathanawat W, Chutinet A, Suwanwela NC, Asdornwised W, et al. Innovations in stroke identification: a machine learning-based diagnostic model using neuroimages. IEEE Access. 2024.
58. Acharya UR, Meiburger KM, Faust O, Koh JEW, Oh SL, Ciaccio EJ, et al. Automatic detection of ischemic stroke using higher order spectra features in brain MRI images. Cognit Syst Res. 2019;58:134–42.
59. Tursynova A, Sakhipov A, Omirzak I, Ikram Z, Smakova S, Kutubayeva M. Classification of Brain strokes in computed tomography images utilizing deep learning. 2024 IEEE 4th International Conference on Smart Information Systems and Technologies (SIST): IEEE; 2024. p. 328–33.
60. Chen J, Zhang J, Xiang J, Yu J, Qiu F. Impact of intelligent convolutional neural network-based algorithms on head computed tomography evaluation and comprehensive rehabilitation acupuncture therapy for patients with cerebral infarction. J Neurosci Methods. 2024;409:110185.
61. Boriesosdick J, Shahzadi I, Xie L, Georgescu B, Gibson E, Frohwein LJ, et al. Deep learning based detection of large vessel occlusions in acute ischemic stroke using high-resolution photon counting computed tomography and conventional multidetector computed tomography. Clin Neuroradiol. 2024;35:1–11.
62. Ahmed Y, Haldar V, Singh T, Saini A. Brain stroke detection using 3D CNN. 2024 2nd International Conference on Disruptive Technologies (ICDT): IEEE; 2024. p. 784–88.
63. Santhi N, Ramasamy N. Unlocking the future of stroke diagnosis-bayesian CNN and MRI fusion. 2024 International Conference on E-mobility, Power Control and Smart Systems (ICEMPS): IEEE; 2024. p. 1–5.
64. Acevedo A, Alférez S, Merino A, Puigví L, Rodellar J. Recognition of peripheral blood cell images using convolutional neural networks. Comput Methods Programs Biomed. 2019;180:105020.
65. Acevedo A, Merino A, Alférez S, Á M, Boldú L, Rodellar J. A dataset of microscopic peripheral blood cell images for development of automatic recognition systems. Data Brief. 2020;30:105474.
66. Bhakte A, Vasista BS, Srinivasan R. Gradient-weighted class activation mapping (Grad-CAM) based explanations for process monitoring results from deep neural networks. 2021 AIChE Annual Meeting: AIChE; 2021.

Publisher's Note